13th International Conference on
Structural Health Monitoring of Intelligent Infrastructure
DOI: 10.3217/978-3-99161-057-1-168

Remote Sensing for Stability Assessment of River Bridges: Case Study of the Red River Bridge in Winnipeg, Canada

D. Cusson[1], H. Stewart[2], C. Regoui[1], J. Zhao[3], K. Helmi[4], B. Telehanic[3], E. Murison[5], D. Thomson[3], A. Mufti[3], S. Clark[3]
[1]National Research Council Canada, Ottawa, Ontario, Canada
[2]Fugro, Houston, Texas, USA
[3]University of Manitoba, Winnipeg, Manitoba, Canada
[4]Arab Academy for Science, Technology and Maritime Transport, Alexandria, Egypt
[5]Manitoba Transportation and Infrastructure, Winnipeg, Manitoba, Canada
Emails: daniel.cusson@nrc-cnrc.gc.ca, hstewart@fugro.com, chaouki.regoui@nrc-cnrc.gc.ca, junhui.zhao@umanitoba.ca, kareem.helmy@gmail.com, telehanb@myumanitoba.ca, evangeline.murison@gov.mb.ca, douglas.thomson@umanitoba.ca, aftab.mufti@umanitoba.ca, shawn.clark@umanitoba.ca

ABSTRACT: With Canada's transportation infrastructure aging, compounded by the effects of climate change, the need to enhance condition assessment through structural health monitoring is increasingly critical to ensure integrity, performance, public safety, and cost-effectiveness. Bridge pier scouring, caused by high river flow and turbulence that erode the surrounding bed material, poses a significant threat to bridge stability and can potentially lead to failure. Conventional scouring inspections are often time-consuming and costly. This paper presents a case study on the Red River Bridge in Winnipeg, Canada, where an innovative, multidisciplinary assessment of bridge stability was performed, including both environmental and structural investigations. The environmental investigation utilized multispectral satellite imagery and optical-band unmanned aerial vehicle (UAV) imagery, combined with large-scale particle image velocimetry (LS-PIV), to assess river flow and turbulence. An anomalous condition near a bridge pier, detected in multispectral satellite imagery, was confirmed by UAV photogrammetry and LS-PIV river current patterns. The structural investigation, detailed in this paper, incorporated Persistent Scatterer Interferometric Synthetic Aperture Radar (PS-InSAR) deformation measurements from satellite imagery, in-situ measurements on the bridge deck, and numerical bridge model predictions. This provided an assessment of the bridge's structural behavior and its potential connection to the condition observed near one of the bridge piers.

KEY WORDS: Satellite PS-InSAR; Remote sensing; Bridge deformation; Case study.

1 INTRODUCTION

1.1 Background and motivation

Canada's transportation infrastructure, especially its bridges, is facing significant challenges due to aging and environmental stresses. Many bridges across the country are nearing the end of their design life, necessitating substantial investments in maintenance and upgrades [1]. The aging infrastructure is further strained by increasing traffic loads and environmental impacts, such as extreme weather events and temperature fluctuations [2]. These factors accelerate the deterioration of bridges, affecting their safety, performance, and economic viability. The need for innovative solutions to ensure long-term sustainability and reliability is more urgent than ever [3].

Bridge pier scouring is a major issue impacting river bridges. It occurs when fast-flowing water erodes the bed material surrounding bridge piers, leading to instability and potential structural failure [4]. This problem is compounded by climate change, which is causing more frequent and severe flooding events [5]. Such conditions accelerate the scouring process, increasing risks to bridge safety and necessitating advanced monitoring and mitigation strategies [6]. Research has shown that various factors, including water velocity, bed material type, and pier shape influence the extent of scouring [7]. Effective countermeasures, such as pier modifications and protective structures, are essential to mitigate these risks [8].

In response to these challenges, there is a growing need to assess bridge safety and performance through structural health monitoring technologies. Remote Sensing for Structural Health Monitoring (RS-SHM) is an emerging field that uses multispectral and radar satellite remote sensing, combined with low-footprint in-situ measurements, to monitor bridge structures between routine inspections. This approach, which does not require bridge closure or create traffic disruption, provides early awareness of developing risks and understanding of how environmental changes may affect structural behaviour and safety. By integrating satellite data with in-situ measurements, engineers can gain comprehensive insights into bridge structural behaviour, enabling proactive maintenance and risk management. This approach enhances safety by providing early detection of risks while improving cost-effectiveness through optimized maintenance plans and extended bridge lifespan.

The integration of advanced sensor technologies and cloud-based platforms in SHM systems allows for continuous real-time monitoring of bridge conditions. These systems can detect even minor structural changes, such as vibrations and displacements, which are critical for assessing the health of aging infrastructure. The use of SHM technologies not only improves the accuracy of bridge assessments but also facilitates timely interventions, thereby preventing catastrophic failures and extending the service life of bridges. As Canada continues to face environmental and economic pressures, the adoption of innovative SHM solutions will be crucial in maintaining the integrity and safety of its transportation infrastructure.

Additionally, the implementation of predictive maintenance strategies, supported by SHM data, can significantly reduce maintenance costs and extend the lifespan of bridge structures, which are typically designed for 75 years in Canada. Predictive maintenance involves analyzing data from SHM systems to forecast potential issues before they become critical, allowing for timely and targeted interventions.

DOI: 10.3217/978-3-99161-057-1-168

This proactive approach enhances safety and optimizes resource allocation, ensuring that inspection, maintenance and rehabilitation efforts are focused on areas with highest risk.

Ultimately, aging transportation infrastructure requires substantial investments to address increasing traffic loads and environmental impacts. Adopting advanced SHM technologies and predictive maintenance strategies offers a promising solution to improve safety, performance, and longevity.

1.2 Case study site

The Red River is a shallow meandering river flowing north through the city of Winnipeg in Manitoba, Canada. The 258-m long Red River Bridge, with four lanes of vehicle traffic and one lane of foot traffic, crosses the Red River south of Winnipeg. Figure 1 shows a satellite view of the bridge, with annotations for bridge piers (P1 to P6), and west and east abutments (WA, EA). Piers P3, P4, and P5 are located in the permanent river channel, while Piers P1, P2, and P6 may become inundated at their base during periods of high flow.

From west to east, the bridge structure consists of a total of seven spans, including two simply-supported spans between WA and P2, where the longitudinal movement is fixed at P1, followed by four continuous spans between P2 and P6, where the longitudinal movement is fixed at P4, and a last simply-supported span between P6 and EA, where the longitudinal movement is fixed at the east abutment. This detail will explain the direction and extent of thermal expansion of deck along the bridge length. Ambient temperature data for this site was acquired from a local weather station located at the Winnipeg international airport, as given in Figure 2.

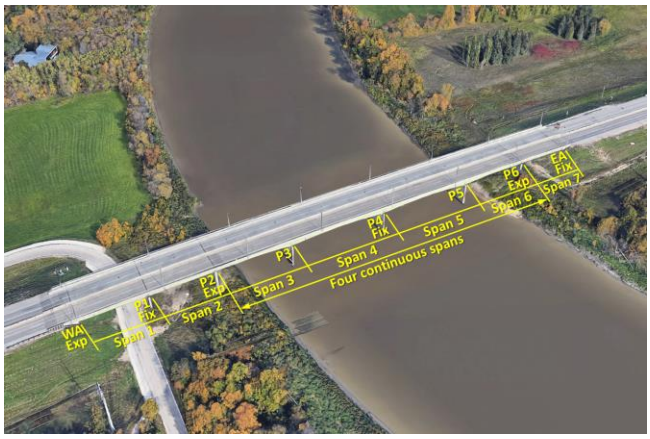

Figure 1. Bridge structure over Red River in Winnipeg, MB.

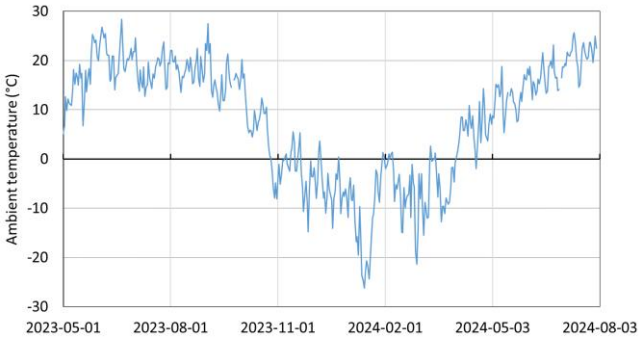

Figure 2. Ambient air temperature measured at Winnipeg international airport during the bridge monitoring period.

2 METHODS

2.1 Environmental investigation summary

In 2023-2024, a multimodal RS-SHM environmental investigation (not yet published) was conducted to detect and monitor potential hazards at the Red River Bridge and its surroundings from multispectral satellite imagery and optical-band UAV imagery. Eight Maxar Worldview mono orthoimage scenes acquired during the ice-free spring and summer months of 2022 were evaluated for river flow conditions that may affect the bridge structure stability. UAV photogrammetry of the riverbanks was conducted in November 2023, and two UAV-based Large Scale Particle Image Velocimetry (LS-PIV) collections were acquired in Spring 2024. These investigations did not require bridge closure or disrupt normal traffic, nor did they necessitate unsafe surveying practices. The findings are used to inform the structural investigation in order to verify if a correlation with the monitored bridge deformations do exist.

2.2 Georeferencing of SAR satellite imagery

Accurate positioning of SAR satellite imagery data, including the integration of up-to-date elevation data, is essential for precise georeferencing during the PS-InSAR analysis [9]. This process ensures that measurements are correctly aligned with real-world coordinates, which is critical for detecting subtle ground deformations. A reliable Digital Surface Model (DSM) plays a pivotal role in this step by accounting for topographic variations. Inaccuracies in the DSM can lead to misplacement of Persistent Scatterers (PS), introducing errors in phase interpretation and ultimately compromising the reliability of deformation estimates. Furthermore, an accurate DSM supports the separation of topographic and displacement signals, enhances phase unwrapping, and improves the 3D localization of PS, particularly in complex urban or mountainous terrains.

The horizontal coordinate reference frame for this project is the North American Datum of 1983 Canadian Spatial Reference System (NAD 83 CSRS). The horizontal geographical units were projected into planar coordinates in the Universal Transverse Mercator (UTM) system, Zone 14 North with a central meridian of 99° W. The vertical coordinate reference system is the Canadian Geodetic Vertical Datum of 2013 (CGVD-2013).

A stereo pair of 50-cm resolution panchromatic-band Airbus Pleiades 1-B satellite images acquired on 14 June 2021 was used to create a 1-m resolution Digital Surface Model (DSM) of the Red River in the Winnipeg metropolitan area, inclusive of the Red River Bridge. Image selection criteria included clear views of the river surface in the vicinity of the bridge, with no clouds, cloud shadows, or aerosols. The source images of the stereo pair were georeferenced using a sparse RTK survey of tie points (bases of lampposts on the pedestrian walkway of the bridge) on the bridge deck conducted by the University of Manitoba with a DJI D-RTK 2 mobile positioning system, orthorectified using the High Resolution Canadian Digital Elevation Model (HR-CDEM), and used to produce the DSM (Figure 3) and image stack with horizontal coordinates and elevations in the project coordinate reference system described previously. Horizontal and vertical accuracies of a DSM derived from satellite imagery in this manner is estimated at +/- 0.5 m horizontal (CE 90) and +/- 1.5 m vertical (LE90) [10].

DOI: 10.3217/978-3-99161-057-1-168

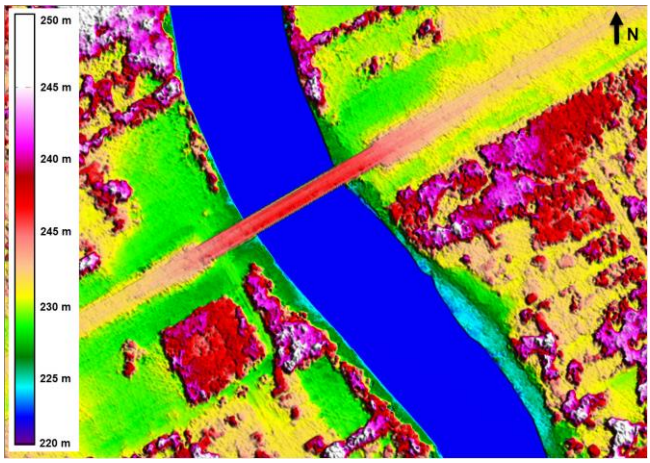

Figure 3. Digital surface model created for the Winnipeg bridge and its surroundings.

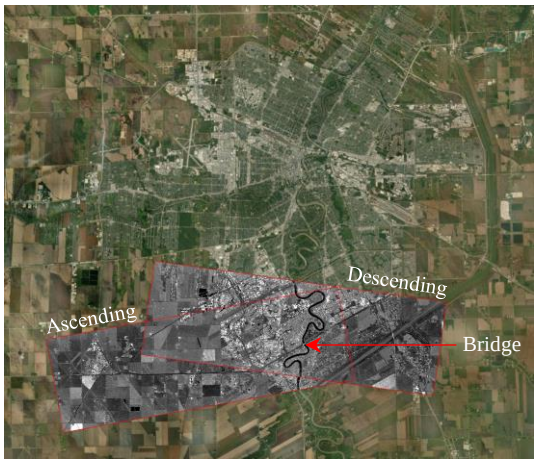

Figure 4. Winnipeg metropolitan area showing footprints of the ascending and descending satellite image stacks.

2.3 PS-InSAR satellite measurements

Persistent Scatterer Interferometric Synthetic Aperture Radar (PS-InSAR) is a satellite-based remote sensing technique used to monitor ground deformation over time. It involves analyzing a series of SAR images acquired at different times to measure the motion of stable ground features (or objects), known as persistent scatterers (PS). This method allows the detection of subtle movements and deformations on the Earth's surface or man-made structures by comparing the phase information (e.g., phase change and intensity) of the radar signals across multiple temporal acquisitions. More details on the PS-InSAR technique are available elsewhere [11][12], along with its applications in preventing bridge collapses [13][14].

The technique was applied to two image stacks of SAR satellite imagery (Figure 4) acquired over the Winnipeg metropolitan area from C-band satellites of the RADARSAT Constellation Mission (RCM), including one stack acquired in ascending viewing geometry (i.e., satellite travelling from south pole to north pole, looking to the East) with an incidence angle of 45° and a satellite track heading of 350°, and a second stack acquired in descending viewing geometry (i.e., satellite travelling from north pole to south pole; looking to the West) with an incidence angle of 42° and a satellite track heading of 190°. The bridge heading angle was measured at 62°. The RCM imaging mode was the Spotlight mode with a nominal pixel resolution of 1 x 3 meters (range vs. azimuth). The minimum and maximum satellite revisit times were four days and twelve days, respectively. The image acquisition period covered in this paper spans approximately one year from May 2023 to June 2024. Table 1 provides the details on the two satellite image stacks processed for this study.

Table 1. Features of RCM satellite image stacks.

Look direction	Ascending	Descending
Beam mode	Spotlight	Spotlight
Incidence angle	45°	42°
Satellite track heading	350°	190°
Resolution (range x azimuth)	1 x 3 m	1 x 3 m
Swath (range x azimuth)	20 x 5 km	20 x 5 km
Number of scenes	29	55
Stack start date	1 May 2023	2 May 2023
Stack end date	16 June 2024	17 June 2024

2.4 In-situ displacement measurements

Figure 1 above illustrates some structural parameters of the bridge, such as the connection details between girders and piers. Permanent survey positions were identified on the bridge deck for the in-situ measurements using a total station (TS) and GPS. These positions were located on the deck and aligned with abutments, piers and mid-spans. Matching markers were added to the metal handrail beside the pedestrian walkway so that the reflection prism for TS and the GPS Antenna could be precisely mounted on the same positions with good repeatability (within +/- 1 mm error) during the measurement period.

The position measurements using the total station were taken from each abutment. The two sitting positions for the TS were fixed, and their origin coordinates were determined using a real-time kinematic (RTK) global positioning system (GPS). The coordinates of the position marks were determined by moving the 360-degree prism from the WA position to the centre of the bridge when the measurements were conducted from the west abutment, and by moving the prism from the EA position to the centre of the bridge when the measurements were taken from the east abutment.

The measurements using the GPS instrument were conducted using a base station and a rover. The base station was mounted at the WA position, and the rover was moved to all positions from WA to EA. The position measurements from the rover can achieve a horizontal positioning accuracy of 6 millimetres with a signal correction from the base station, while a vertical positioning accuracy of 10 millimetres can be achieved. The RTK correction signal was communicated between the rover and the base using a radio link. To ensure accuracy, data were collected with correction times of 1-2 seconds. The thermal movement of the marked positions on the handrail was measured against temperature during a period of a few months.

2.5 Numerical bridge model simulations

Figure 5 shows the finite element model (FEM) of the bridge using the SAP 2000 software, assuming linear elastic material behaviour. It was used to study the dynamic vibrations of the bridge and the ambient temperature dependence of bridge displacements. The bridge's steel girders and concrete slab were modelled using thin shell elements connected by stiff link elements.

DOI: 10.3217/978-3-99161-057-1-168

The bracing system, brackets, and edge beams supporting the sidewalk were modelled using frame elements. The bridge abutments were modelled using thick shell elements, and the bearings between abutments and girders were modelled with special link elements to allow rotation only or rotation and relative displacement depending on bearing type.

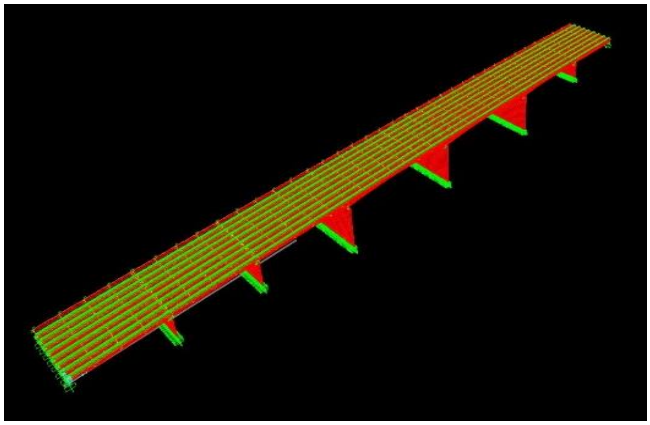

Figure 5. The numerical finite element model of the bridge.

An element size of up to 600 mm was chosen after comparing the results from several mesh sizes for a portion of the bridge. The complete model consists of 85,526 nodes, 2,268 frame elements, 6,912 thick shell elements, 75,133 thin shell elements and 12,704 link elements.

A FEM simulation is a component of a digital twin, but it does not constitute a digital twin on its own. Our work extends beyond the mere simulation by continuously updating and predicting the structure's performance using real-time data. Human intervention plays a crucial role in this process, modifying results by comparing outputs from FEM simulations, remote satellite imagery, and in-situ GPS, and TS.

3 RESULTS AND ANALYSES

3.1 Environmental observations

The findings of this case study demonstrate how spatio-temporal environmental information is used to provide context to bridge deformation measurements in an RS-SHM study. Unexpected river turbulences observed in three different datasets (mono ortho satellite imagery, UAV imagery, LS-PIV vectors) acquired over a 2-year period indicate the presence of unexpected river behaviour upstream of Pier P5. The very high-resolution UAV photogrammetry collection provided particularly interesting contextual information for PS-InSAR monitoring, notably that riverbank sediment loss was occurring upstream of the bridge and a persistent pile of woody debris was present at the base of Pier P5 in all LS-PIV video collections but not at any other piers. The LS-PIV results confirmed the presence of a subsurface obstruction to river flow observed in the satellite image stack and revealed an area of unexpectedly high currents near the east bank of the river. These observations are sufficient to indicate that more detailed assessment of pier stability using other methods is required.

3.2 PS-InSAR displacement results

PS-InSAR analysis was conducted independently on each stack of ascending and descending satellite images. The resulting time series include measurements projected in the one-dimensional line-of-sight (LOS) of the satellite.

Three types of displacement measurements were obtained: (i) displacement linear rate (or velocity) derived from linear regression against time, (ii) displacement thermal sensitivity (or unit thermal displacement) obtained from linear regression against ambient temperature taken at times of image acquisitions, and (iii) cumulative displacements over the acquisition period (one year so far).

Figure 6 illustrates the ascending (top) and descending (bottom) sets of LOS linear displacement rates measured over the bridge deck, where the bridge concrete barriers with steel railings are perfect natural reflectors of SAR energy. However, due to the shallow incidence angle and the satellite look direction, not all sections of the barriers reflected valid persistent scatterers. Most ascending-pass PS concentrated on the north-west barrier while most descending-pass PS concentrated on the south-east barrier, making it challenging for the 2D decomposition analysis (explained next). Nevertheless, the study of these datasets reveals no excessive LOS displacement linear rates observed in the ascending or descending satellite data. Different viewing geometries (i.e., ascending and descending) were specifically selected to allow for a 2D decomposition calculation of the vertical and horizontal (east-west) components of displacement, noting that pole-orbiting satellites are not sensitive to pure north-south movement [11][12].

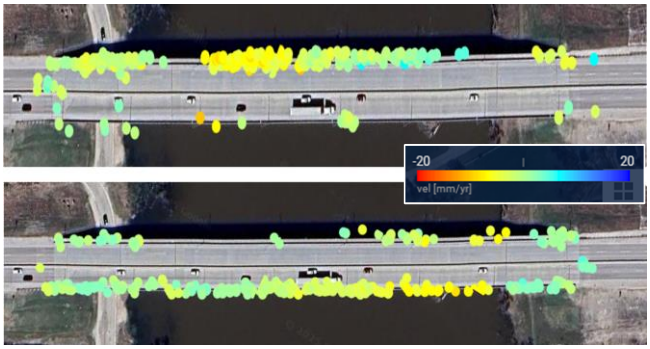

Figure 6. PS-InSAR LOS displacement linear rates (mm/year) measured over the bridge deck from ascending viewing geometry (top) and descending viewing geometry (bottom).

Figure 7 shows a horizontal grid of nine consecutive bins along the deck centreline, which was used for averaging displacement measurements from each viewing geometry. The bins were used to calculate the average vertical and horizontal components of displacement at the centre of each bin by trigonometry. The size of the bins was carefully selected to get representative values of displacement for each span of the bridge considering the different support conditions at the piers and abutments (free, pinned or fixed). The advantage of large bins is that each bin can contain multiple persistent scatterers from both ascending and descending satellite passes, enabling accurate 2D decomposition. A 2nd set of 18 consecutive bins was also created for comparison purposes, where the length of each bin was exactly half that of the 1st set (i.e., 14.4 m), with the aim to get a well-distributed set of average displacements, perhaps at the expense of having a few empty bins for either ascending or descending viewing geometry.

DOI: 10.3217/978-3-99161-057-1-168

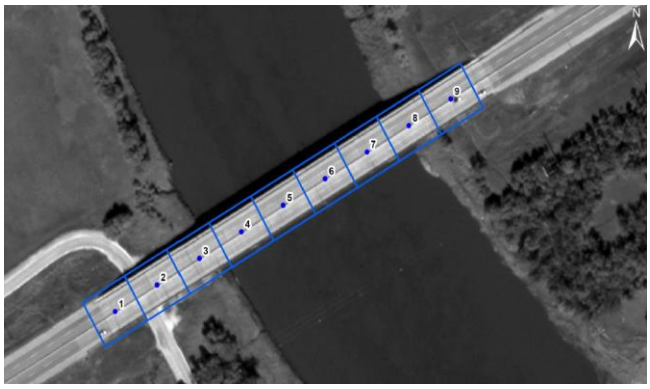

Figure 7. 2D decomposition grid over the bridge deck, showing nine regularly-spaced bins. Each bin is 28.8 m long.

Figure 8 illustrates how 1D LOS displacement measurements from two opposite satellite viewing geometries can be combined for a 2D decomposition of the vertical and horizontal components of displacement.

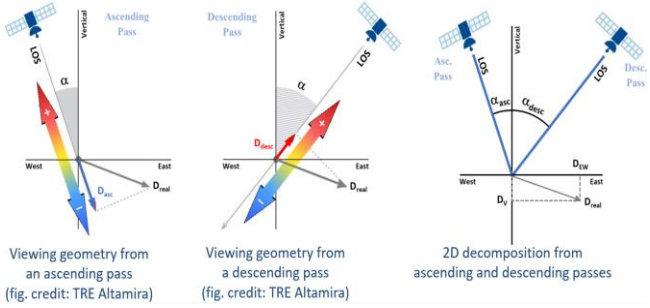

Figure 8. Satellite viewing geometries and 2D decomposition.

Equation 1 was adapted for a bridge-centric coordinate system [15]. If both the vertical and transverse components of displacement can be assumed to be small compared to the longitudinal component, then Equation 1 can reduce to Equation 2. The east-west component of displacement can then be projected onto the longitudinal direction of the bridge for direct comparison with other measurement and prediction methods. Similarly, if both longitudinal and transverse components of displacement can be assumed to be small in comparison to the vertical component, then Equation 1 can reduce to Equation 3, as follows:

$$D_{LOS} = D_V \cos\alpha - D_L \sin\alpha \sin\beta + D_T \sin\alpha \cos\beta \quad (1)$$

$$D_L = -D_{LOS}/(\sin\alpha \sin\beta) \quad \text{if both } D_V \text{ and } D_T \sim 0 \quad (2)$$

$$D_V = D_{LOS}/(\cos\alpha) \quad \text{if both } D_L \text{ and } D_T \sim 0 \quad (3)$$

where D_{LOS} is the line-of-sight displacement toward the satellite sensor, D_V is the vertical component in the upward direction, D_L is the horizontal component in the longitudinal direction of the bridge from west to east, D_T is the horizontal component in the transverse direction of the bridge, α is the incidence angle of the satellite LOS, and β is the angle measured clockwise from the satellite track heading to the bridge longitudinal axis.

However, if the vertical and transverse components of displacement are not negligible, Equation 4 should be used to calculate the longitudinal displacement:

$$D_L = \left[\frac{D_{LOS,d}}{\cos\alpha_d \tan\alpha_a \sin\beta_a} - \frac{D_{LOS,a}}{\sin\alpha_a \sin\beta_a}\right] \Big/ \left[1 - \frac{\tan\alpha_d \sin\beta_d}{\tan\alpha_a \sin\beta_a}\right] \quad (4)$$

Similarly, if the longitudinal and transverse components of displacement are not negligible, Equation 5 should be used to calculate the vertical displacement:

$$D_V = \left[\frac{D_{LOS,d}}{\cos\alpha_d} - D_{LOS,a}\frac{\tan\alpha_d \sin\beta_d}{\sin\alpha_a \sin\beta_a}\right] \Big/ \left[1 - \frac{\tan\alpha_d \sin\beta_d}{\tan\alpha_a \sin\beta_a}\right] \quad (5)$$

where subscripts a and d represent the components calculated from the ascending or descending image stacks, respectively.

3.3 Comparison between PS-InSAR and other methods

In-situ measurements were conducted on the bridge, as described previously in Section 2.4. The distances from all marks to Mark 1 (located at the west abutment) were calculated, and the distance changes against ambient temperature variation during the measurement period were obtained (Figure 9). It can be seen that both in-situ measurement methods agree well with each other and to the FEM predictions of unit thermal displacement along the bridge, as expected. A small 0.2 mm/°C mean error is observed between the two sets of in-situ measurements and the FEM predictions.

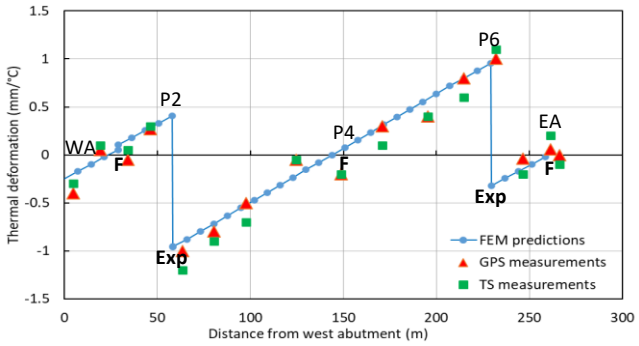

Figure 9. In-situ thermal displacements of bridge along the longitudinal direction compared to FEM predictions. (Notation: F = fixed joint; Exp = expansion joint).

In addition, the bridge unit thermal displacement in the vertical direction was also predicted with the FE model and measured with the total station and GPS instruments, for which the results are presented in Figure 10.

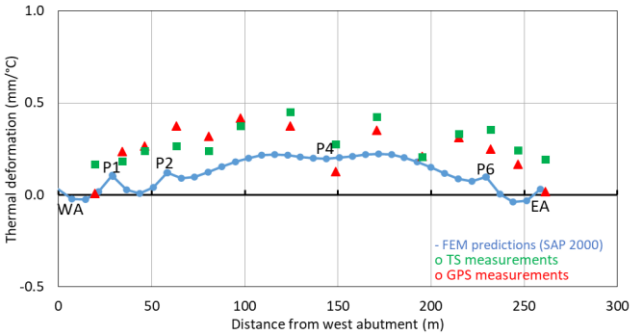

Figure 10. In-situ thermal displacements of bridge along the vertical direction compared to FEM predictions.

DOI: 10.3217/978-3-99161-057-1-168

It can be observed that both types of field measurements agree well with the FEM predictions of vertical displacement.

Given that the FEM predictions of thermal displacements appear to be valid based on the horizontal and vertical field measurements, the PS-InSAR measurements will be compared to and validated against the FEM predictions in the next figures.

Figure 11 illustrates the average longitudinal thermal displacement measured by the RCM satellites for each set of bins along the bridge deck from West to East, using the detailed Equation 4. The expected movement direction (eastward vs. westward) and extent of thermal displacement are well characterized, with gradually increasing thermal displacements between the two expansion joints (at P2 and P6) and the expected sign reversal on either side of each expansion joint due to opposite directions of thermal movement going away from the pier. The comparison between the thermal displacements obtained from each bin size illustrates excellent agreement between the results of the two bin sizes, except that the smaller bin size returned no data at two locations near P6.

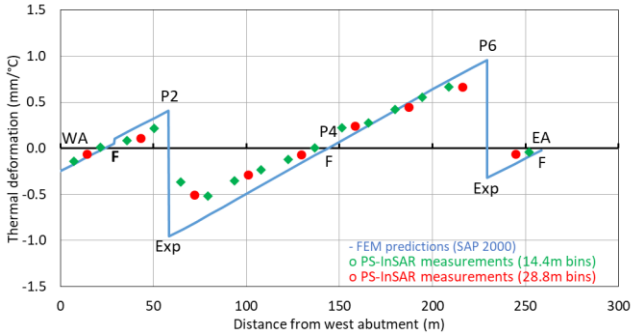

Figure 11. PS-InSAR thermal displacement along the longitudinal direction of bridge compared to FEM predictions.

Similarly, Figure 12 illustrates the PS-InSAR data for the vertical component of thermal displacement calculated along the bridge using Equation 5 for the two sets of bins. The comparison from either set of bins with the FEM predictions shows a good match, where the difference ranges from 0.1 mm/°C to 0.2 mm/°C. These PS-InSAR measurements also compare very well with the field measurements in Figure 10 above.

Overall, the satellite-monitored bridge thermal displacements are observed to be consistent with and very similar to both in-situ measurements and FEM predictions, confirming satellite-based PS-InSAR as a promising SHM tool for displacement measurements.

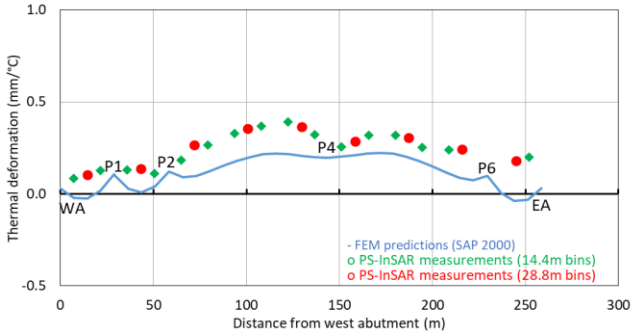

Figure 12. PS-InSAR thermal displacement along the vertical direction of bridge compared to FEM predictions.

3.4 Assessment of PS-InSAR calculation method accuracy

As mentioned in the previous section, the PS-InSAR measurements of the longitudinal thermal displacement shown in Figure 11 were calculated using Equation 4. These results show a maximum difference of 0.3 mm/°C at the expansion peaks (P2 and P6) compared with the FEM predictions. This difference is believed to be due to an averaging effect from the relatively large size of the bins used for 2D decomposition, especially around the P2 and P6 discontinuities. Shorter averaging bins would have been desired if the density of the ascending PS on the downstream barrier and the descending PS on the upstream barrier were higher (Figure 6). At P3 and P5, where the averaging effect is negligible, a small difference of 0.2 mm/°C is observed when compared to the FEM predictions.

Table 2 presents standard deviation and point count statistics for the PS results obtained from the 2D decomposition depending on pass direction and bin size. It is shown that the bin size did not have a significant impact of the accuracy of the averaged results, except that the smaller bin size had two empty bins around P6 due to the low density of PS for the ascending pass. The ascending data exhibited slightly higher standard deviations than the descending data, which is likely due to the lower PS density in the ascending pass, which also had fewer images in its stack (29 vs. 55, as shown in Table 1) compared to the descending stack.

Table 2. Standard deviation and point count statistics for PS-InSAR results from ascending and descending passes.

Bin no.	Bin centre distance from WA (m)	Ascending pass		Descending pass	
		St. dev. within each bin (mm/°C)	PS point count in each bin	St. dev. within each bin (mm/°C)	PS point count in each bin
9-bin grid:					
1	14.4	0.09	42	0.08	37
2	43.2	0.07	24	0.09	24
3	72.0	0.10	16	0.08	25
4	100.8	0.09	55	0.07	47
5	129.6	0.11	27	0.04	27
6	158.4	0.07	40	0.06	41
7	187.2	0.10	24	0.05	30
8	216.0	0.01	2	0.03	15
9	244.8	0.05	5	0.07	43
18-bin grid:					
1a	7.20	0.10	19	0.05	19
1b	21.6	0.07	23	0.05	18
2a	36.0	0.07	21	0.04	16
2b	50.4	0.01	3	0.13	8
3a	64.8	-	1	0.12	11
3b	79.2	0.10	15	0.05	14
4a	93.6	0.09	25	0.04	19
4b	108.0	0.08	30	0.06	28
5a	122.4	0.07	15	0.04	10
5b	136.8	0.11	13	0.03	17
6a	151.2	0.06	27	0.05	24
6b	165.6	0.08	13	0.04	17
7a	180.0	0.09	18	0.05	23
7b	194.4	0.05	5	0.04	7
8a	208.8	0.01	2	0.03	10
8b	223.2	-	0	0.04	5
9a	237.6	-	0	0.04	13
9b	252.0	0.05	5	0.07	30

DOI: 10.3217/978-3-99161-057-1-168

This study was fortunate to have access to two stacks of satellite imagery over the bridge from opposing viewing geometries, which allowed the full 2D decomposition of movement for the correct determination of horizontal (east-west) and vertical components of movement. This is convenient when one needs to compare and validate results with field measurements and/or numerical simulations for which displacement results are typically determined in the vertical and horizonal directions.

There are cases where satellite imagery is only available for one viewing geometry (ascending or descending). While it is possible to estimate the horizontal or vertical displacement components by simple trigonometry (Equation 2 or 3, for example), one needs to ensure that the unknown variable is small enough to be safely neglected. Case studies on SAR satellite-monitored highway bridges have been successfully conducted using SAR imagery obtained only from one viewing geometry [16][17].

In this study, however, it was found that the vertical component of displacement could not be neglected. For example, Figure 13 presents the PS-InSAR measurements of unit thermal displacement in the longitudinal direction of the Red River Bridge, which were calculated separately for each viewing geometry using the simplified Equation 2, which comes with the assumption of negligible vertical displacement. The results actually show a poor match with the FEM predictions, especially for the descending set of displacement data, where differences with the FEM predictions of up to 0.8 mm/°C can be observed.

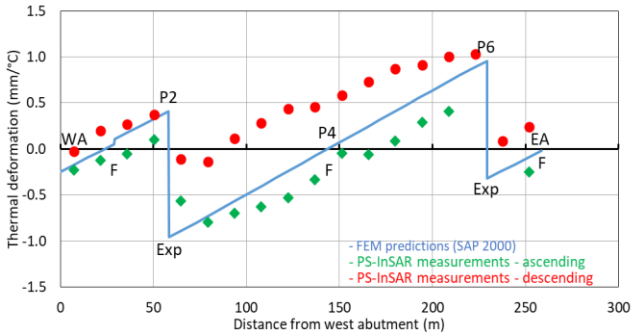

Figure 13. Longitudinal PS-InSAR thermal displacement for either ascending or descending passes compared to FEM predictions, using the inappropriate assumption of negligible vertical displacements. Dotted lines indicate lack of PS data.

The inferior match with the FEM predictions for the descending image stack is unique to this case study and depends on several factors – one of them being the orientation of the bridge with respect to the satellite tracks on the ground. As mentioned earlier, SAR satellites are not sensitive to movement along the satellite track heading (roughly N-S). This is because they are typically right-looking polar-orbiting satellites.

In this study, the angle between the satellite look direction (satellite track heading + 90°) and bridge heading is much larger for the descending stack (190°+90°−62°=218°) than it is for the ascending image stack (350°+90°−62°−360°=18°). Consequently, the ratio of vertical movement to the reduced observable longitudinal movement from the descending viewing geometry becomes apparently larger. This confirms the fact that SAR satellites are most sensitive to movement aligned with the look direction of the satellite [11][12].

3.5 Interpretation of results based on environmental context

As mentioned in the introduction section, the RS-SHM approach is meant to provide bridge operators with early awareness of developing risks and context to understand how changes in the surrounding environment may affect structural behaviour and safety.

The environmental investigation actually identified such a risk to bridge stability: a subsurface bluff-body obstruction to river flow and unexpectedly high currents near the east bank of the river close to Pier P5 of the bridge. These observations were sufficiently significant and clear to trigger a more detailed structural assessment of bridge stability using other methods.

The structural investigation, indeed, focused on two major aspects of structural behaviour of the bridge. The first aspect included the vibration measurements of bridge piers reported elsewhere [18]. The vibration study identified the fundamental natural vibration frequencies of the bridge piers and will keep monitoring them to detect changes where a reduction of the fundamental natural frequency is expected to indicate the weakening of the pier foundation as a result of scouring. Damping is another indicator but is not being considered.

The second aspect of the structural investigation included the thermal behaviour of the bridge, which was obtained by four different measurements and prediction methods (PS-InSAR, TS, GPS and FEM). The remote PS-InSAR and in-situ measurement methods agreed well with the expected bridge thermal deformation predictions from the bridge FE model.

Given the above, there is currently no evidence or signs of pier scouring at the bridge. However, due to observations from the environmental investigation, the deformations and ambient vibrations of the bridge piers, particularly at Pier 5, will remain under close scrutiny.

4 CONCLUSIONS

As part of a case study conducted on the Red River Bridge in Winnipeg, Canada, a structural investigation combining PS-InSAR deformation measurements from satellite imagery, in-situ measurements on the bridge deck, and numerical bridge model predictions was conducted. It provided an assessment of the bridge's structural behaviour with insight obtained from a prior environmental investigation. The following conclusions can be drawn:

1. This case study demonstrated the importance of combining key environmental observations with structural health monitoring data in an RS-SHM approach to provide comprehensive risk assessments for river bridges.
2. The environmental investigation identified unexpected river behaviour, including riverbank sediment loss, flow contraction during high-water periods, and persistent woody debris near Pier P5 of the bridge, suggesting potential risks to bridge stability, thus warranting further assessment of pier stability.
3. PS-InSAR displacement measurements were found to be consistent with in-situ and numerical model predictions, confirming its reliability as a monitoring tool, and have proven effective in this case study for assessing bridge stability and detecting subtle deformations over time.

DOI: 10.3217/978-3-99161-057-1-168

4. The successful 2D decomposition of PS-InSAR displacement data allowed for accurate determination of both vertical and horizontal components, emphasizing the value of having satellite imagery from two opposing satellite viewing geometries.
5. It was demonstrated that, under some specific conditions, analyzing SAR images from only one viewing geometry might induce measurement inaccuracies if the simplifying assumptions on expected displacements cannot be met.
6. Although no current evidence of scouring was detected, the findings of the environmental investigation highlight the importance of remaining vigilant due to the potential scouring risks observed at Pier P5.

ACKNOWLEDGMENTS

The PS-InSAR work detained in this paper has been supported by collaborative research funding from the National Research Council Canada's Artificial Intelligence for Logistics Program with funding from Defence Research and Development Canada's Canadian Safety and Security Program (DRDC/CSSP).

The environmental investigation summarized in this paper was financially supported by the National Research Council Canada's Initiative on Climate Resilient Built Environment.

The authors would also like to acknowledge the Canadian Space Agency for providing the RCM satellite imagery and TRE Altamira for performing the PS-InSAR analysis.

The work related to the in-situ bridge displacement measurements and numerical bridge simulations was conducted by SIMTReC at the University of Manitoba, which was financially supported by the National Research Council Canada and Manitoba Transportation and Infrastructure.

REFERENCES

[1] Transport Canada, Overview of Canada's Transportation Sector, 2021. Retrieved from Transport Canada.
[2] Transport Canada, Outlook, Trends and Future Issues, 2011. Retrieved from Transport Canada.
[3] Senate Committee on Transport and Communications, Critical Transportation Infrastructure Vulnerabilities Place Lives and Economy at Risk, 2024. Retrieved from Senate of Canada.
[4] A. Baranwal, B.S. Das, Scouring Around Bridge Pier: A Comprehensive Analysis of Scour Depth Predictive Equations for Clear-water and Live-bed Scouring Conditions, Journal of Water Supply: Research and Technology-Aqua, 73(3), 2024.
[5] R. Farooq, A.R. Ghumman, Impact Assessment of Pier Shape and Modifications on Scouring around Bridge Pier, Water, 11(9), 2019.
[6] Kistler Group, Structural Health Monitoring (SHM), 2024. Retrieved from Kistler.
[7] P. Dubey, Bridge Protection and Traffic Safety at Its Finest. Informed Infrastructure, 2024. Retrieved from Informed Infrastructure.
[8] Smartec, Bridge Structural Health Monitoring Systems, 2024. Retrieved from Smartec.
[9] H. Stewart, D. Cusson, Digital Surface Models from Satellite Imagery for Improving the Geolocation of InSAR Deformation Measurements on Bridge Structures, 7th International Conference on Smart Monitoring, Assessment and Rehabilitation of Civil Structures (SMAR), Salerno, Italy, 4-6 September, 2024.
[10] Airbus Defense and Space, 202 Pleiades Neo User Guide, V3.0, Toulouse, France, 2021.
[11] M. Crosetto, O. Monserrat, M. Cuevas-González, N. Devanthéry, B. Crippa, Persistent Scatterer Interferometry: A review. SPRS Journal of Photogrammetry and Remote Sensing, 115, 2016.
[12] A. Ferretti, A. Monti-Guarnieri, C. Prati, F. Rocca, D. Massonnet, InSAR Principles: Guidelines for SAR Interferometry Processing and Interpretation, European Space Agency Publication TM-19, Noordwijk, The Netherlands, 2007.
[13] S. Selvakumaran, S. Plank, C. Geiß, C. Rossi, C. Middleton, Remote Monitoring to Predict Bridge Scour Failure Using Interferometric Synthetic Aperture Radar (InSAR) Stacking Techniques, International Journal of Applied Earth Observation and Geoinformation, 73, 2018.
[14] P. Milillo, G. Giardina, D. Perissin, G. Milillo, A. Coletta, C. Terranova, Pre-Collapse Space Geodetic Observations of Critical Infrastructure: The Morandi Bridge, Genoa, Italy, Journal of Remote Sensing, 11, 2019.
[15] S. Samieie-Esfahany, R.F. Hanssen, K. van Thienen-Visser, A. Muntendam-Bos, On the Effect of Horizontal Deformation on InSAR Subsidence Estimates, Fringe 2009, Frascati, Italy, Nov. 30–Dec. 4, 2009.
[16] D. Cusson, H. Stewart, Satellite Synthetic Aperture Radar, Multispectral, and Infrared Imagery for Assessing Bridge Deformation and Structural Health – A Case Study at the Samuel de Champlain Bridge, Journal of Remote Sensing, 16(4), 2024.
[17] D. Cusson, C. Rossi, I. Ozkan, Early Warning System for the Detection of Unexpected Bridge Displacements from Radar Satellite Data. Journal of Civil Structural Health Monitoring, 11, 2020.
[18] J. Zhao, K. Helmi, B. Telehanic, E. Murison, D. Cusson, C. Regoui, A. Mufti, D. Thomson, Bridge scour Detection and Displacement Monitoring using Vibrational Analysis and Radar Satellite Imagery, CSCE Structures Specialty Conference, Winnipeg, Canada, May 28-30, 2025.